Submitted to small NANO MICRO

Supporting Information

Tearing graphene sheets from adhesive substrates produces tapered nanoribbons

Dipanjan Sen, Kostya S. Novoselov, Pedro Reis, and Markus J. Buehler [*]

[*] Prof. M. J. Buehler, Dipanjan Sen
Laboratory for Atomistic and Molecular Mechanics, Department of Civil and Environmental Engineering, Massachusetts Institute of Technology,
77 Massachusetts Ave., Room 1-235A&B, MA 02139 (USA)
E-mail: mbuehler@mit.edu (corresponding author)
Dr. Kostya Novoselov
School of Physics & Astronomy, University of Manchester,
Manchester M13 9PL (UK)
Dr. Pedro M. Reis
Department of Mathematics, Massachusetts Institute of Technology,
77 Massachusetts Ave., Cambridge, MA 02139 (USA)

Model for elastic-stretching dominated tearing mechanics

From the molecular dynamics simulations results presented in Figure 3a of the main text (plot of the sine of half of the tearing angle, $\sin(\theta/2)$, versus square root of the adhesion strength, $\sqrt{\tau}$), we conclude that there are two regimes in the tearing process of the graphene sheets. Moreover, the calculated atomistic stress fields in the adhered sheet close to the tear ridge shown in Figure 4 in the main text, suggest an increasing contribution of elastic stretching energy to the system energy at higher adhesion strengths. This indicates the existence of the two regimes correspond to bending-energy-dominated (at low adhesion strengths, $2 < \tau < 8$ J m^{-2}) and stretching-energy-dominated (at high adhesion strengths, $\tau > 8$ J m^{-2}) tearing.

Whereas the regime where bending energy dominates has been previously considered in the literature,[21] the corresponding theory for the stretching dominated tearing has still to be developed. The previous continuum theory[21] accounts for the release of elastic bending energy in the fold joining the two tears as the tears move forward. The bending energy is released by the simultaneous advancement of the crack tips in the Y direction and their approximation in the X direction, thereby reducing the width of the ridge. In this Supplementary Information we modify the previous model,[21] to account for the new loading and boundary conditions under which elastic stretching energy in the flap and adhered sheet become large in comparison to the bending energy and its contribution can no longer be neglected.

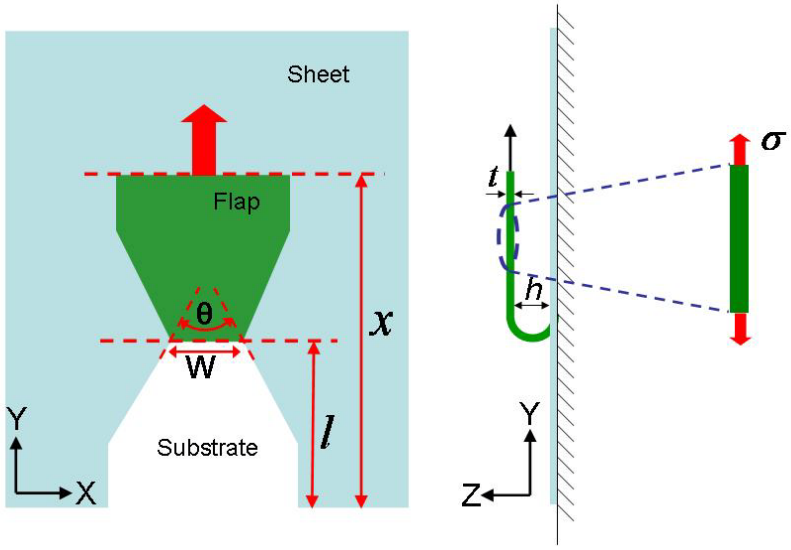

Figure S1. A schematic drawing showing the setup for the tearing studies of graphene. The plot shows a top view and side view. An initial flap is cut in the sheet, folded back and moved at a constant speed. The thickness of the sheet is t. The distance h gives the height of the fold. W is the width of the fold at the adhesion edge, l and x are the distances from the bottom edge of the sheet to the fold and flap edge respectively. θ is the angle of tearing. The zoomed in view on the right side shows a section of the flap and the action of the stretching stress in the flap.

First, we seek a relation between stretching force in the flap and adhered sheet and adhesion strength to the substrate. The total energy of the system can be split as, $U = U_E + 2\gamma ts + \tau A$, where the terms correspond to elastic energy, fracture energy and adhesion energy, respectively. Here, t is the graphene sheet nominal thickness, s is the length of the crack, γ is the work of fracture of the film per unit cross-sectional area, and τ is the adhesive energy per unit surface area of interface, and A and 2ts are the peeling and tearing surface areas, respectively (Figure S1). The elastic energy itself can be split as, $U_E = U_{bend} + U_{stretch}$, where the two terms correspond to bending energy (associated in the bent cylindrical ridge) and stretching energy (stored in the flat portion of the flap and the adhered sheet). In the remainder of this document, the part of the sheet being torn off and bent back is referred to as the flap, and the rest of the adhered sheet is referred to as the flat sheet.

In contrast to the earlier continuum analysis,[21] from the atomistic simulations we find that the height of the fold, h, changes during the bending-dominated regime as a function of the adhesion energy, whereas it remains approximately constant as a function of adhesion energy in the stretching-dominated regime. This implies that the contribution from bending energy becomes constant once stretching dominates. As such, bending can be regarded as a constant contribution to the total stored elastic energy. This total stored elastic energy can then be written as a function of the stretch in the flap as, $U_E = U_E(x - l, W)$. In a displacement controlled experiment, the first variational of the total energy, U, with respect to the various geometric parameters is,

$$\delta U = \left(\partial_W U_E\right)_{x,l} \delta W + \left(\partial_l U_E\right)_{x,W} + 2\gamma t \delta s + \tau W \delta l \,. \qquad \text{(S1)}$$

In addition, the applied force is given by the work theorem as $F = \left(\partial_x U_E\right)_{l,W}$. Using this relation for the force, along with the condition for mechanical equilibrium of the system,[56] $\partial U / \partial s = 0$, from Equation (S1), we get

$$F\cos\frac{\theta}{2} = 2\gamma t + \tau W\cos\frac{\theta}{2} - 2\left(\partial_W U_E\right)_{x,l}\sin\frac{\theta}{2}. \quad \text{(S2)}$$

To obtain the angle of crack propagation, we apply the maximum energy release-rate criterion,[56] $\partial_\theta\left(\delta U/\delta s\right) = 0$, which using Equation (S2) yields,

$$F\sin\frac{\theta}{2} = \tau W\sin\frac{\theta}{2} + 2\left(\partial_W U_E\right)_{x,l}\cos\frac{\theta}{2}. \quad \text{(S3)}$$

These equations can be simplified to,

$$F = \tau W + 2\gamma t\cos\frac{\theta}{2},$$
$$\left(\partial_W U_E\right)_{x,l} = \gamma t\sin\frac{\theta}{2}, \quad \text{(S4)}$$

by projection onto the X-Y coordinate system (see Figure S1).

Up to this point, the analysis is identical to that of Hamm et al[21] but now we consider the contribution due to stretching of the straight portion of the flap, and of the adhered sheet ahead of the bent edge.

The applied force can be calculated from the stretching strain in the flap, as, $F = \sigma Wt = E\varepsilon Wt$. When the width is large, such that $\tau W >> \gamma t$, we get, from Equation (S4), $F \approx \tau W$, and thus,

$$\varepsilon \approx \tau/Et. \quad \text{(S5)}$$

This predicts a linear relation between strain in the flap, ε, and the adhesion energy, τ. Both of these quantities can be easily measured in the atomistic simulations and are plotted in Figure S2. The value of $1/Et$ for graphene modeled by ReaxFF[30] is 0.0025 m^2 J^{-1}. A linear square fit to the $\varepsilon(\tau)$ numerical data yields a slope of 0.0018±0.00005 m^2 J^{-1}, which is consistent, and of the same order of magnitude as the predicted value.

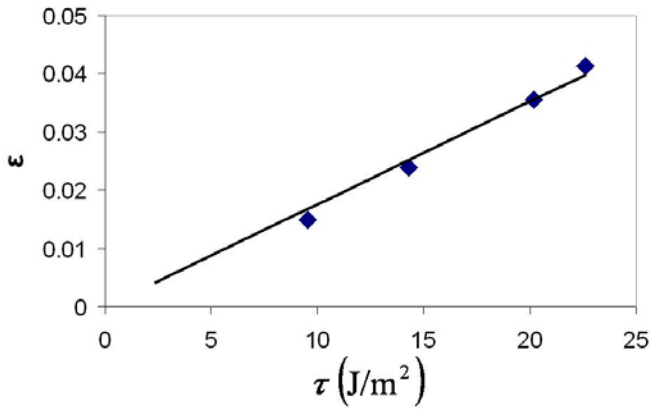

Figure S2. Tensile strain ε_{yy} in the flap measured as a function of the adhesion strength from molecular dynamics experiments. Pulling speed is held constant. The slope of the linear fit is 0.0018±0.00005 m^2 J^{-1}.

To obtain the angular dependence of the tearing on the adhesion strength, we need an estimate of the elastic energy stored both in the sheet and in the flap (second part of Equation S4), as follows. Consider an infinite isotropic material with two semi-infinite cracks parallel to each other, separated by a width W. Let the strip be under far-field uniform plane stress $\sigma_{xx} = \sigma$ (Figure S3).

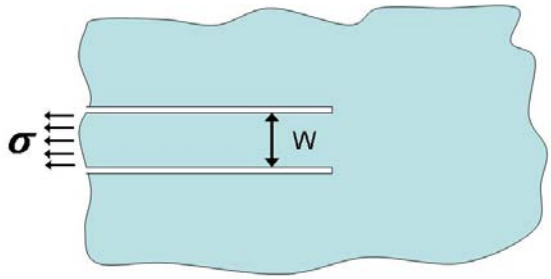

Figure S3. Schematic of an infinite sheet with two semi-infinite cracks, separated by W. The strip of material between the cracks in under a far-field tensile stress of σ.

The energy release rate under this loading predicted by energy balance using linear elastic fracture mechanics is:[57]

$$G_{stretch} = \frac{\sigma^2 W}{4E}. \qquad \text{(S6)}$$

The stretching configuration in our tearing experiments resembles this geometry and loading conditions. Our system is however different from this idealized system for the following reasons: a) the finite size of the crack, and (b) the finite dimensions of the sheet. The effect of these two geometric factors, i.e. finite surface crack and finite specimen dimensions, can be grouped into a dimensionless numerical factor f, so that,

$$G_{stretch} = f\frac{\sigma^2 W}{4E}. \qquad \text{(S7)}$$

This is the energy release rate per unit thickness and per unit length advance of the crack and by integrating over the crack length and thickness of sheet, we obtain,

$$U_{stretch} = f\frac{\sigma^2 W}{4E} lt + U_{stretch}^{no\,crack}(W), \qquad \text{(S8)}$$

where $U_{stretch}^{no\,crack}(W)$ is the stretching energy stored in the sheet under external load when no crack is present, and is a function of W alone.

To calculate the second term in Equation (S8), we consider a semi-infinite thin plate under an edge load of magnitude $\sigma W t$, as shown schematically in Figure S4.

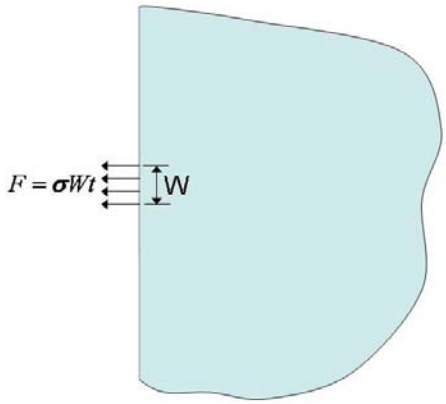

Figure S4. Schematic of a semi-infinite thin plate under a load F spread over a width W on the edge.

For points on the plate far away from the location of the applied load, this load can be considered as a point force. In that case, according to linear elasticity theory[52] the displacement field far away from the load application is,

$$u \propto \frac{F}{Et} = \frac{\sigma W}{E}. \tag{S9}$$

Hence, the strain energy stored in the plate scales as $U_{stretch}^{no\,crack} = \beta \frac{\sigma^2 W^2 t}{E}$, where β is a dimensionless numerical prefactor. Thus, the total stretching energy, from Equation (S8), is,

$$U_{stretch} = f \frac{\sigma^2 W}{4E} lt + \beta \frac{\sigma^2 W^2 t}{E}. \tag{S10}$$

The relation between the applied far-field stress and the adhesion energy (Equation S5) can now be substituted into Equation (S10) to obtain the adhesion strength dependence of the elastic stretching energy as,

$$U_{stretch} = \left(f \frac{Wlt}{4} + \beta W^2 t \right) \frac{\tau^2}{Et^2}. \tag{S11}$$

Finally, when the contribution from stretching energy dominates the elastic energy in the sheet, the second part of Equation (S4) becomes,

$$\gamma t \sin\frac{\theta}{2} = \left(\partial_W U_E\right)_{x,l} \approx \left(\partial_W U_{stretch}\right)_{x,l}, \tag{S12}$$

and after rearrangement, we arrive to an expression that relates the sine of half of the tearing angle with the various geometric and material properties of the system:
Or,

$$\sin\left(\frac{\theta}{2}\right) \approx \left(\frac{fl}{4} + 2\beta W \right) \frac{\tau^2}{\gamma E t^2}. \tag{S13}$$

After calculating mean values we obtain,

$$\left\langle \sin\left(\frac{\theta}{2}\right) \right\rangle \approx \left(\frac{f\bar{l}}{4} + 2\beta \overline{W} \right) \frac{\tau^2}{\gamma E t^2} \propto \tau^2, \tag{S14}$$

where $\left\langle \sin\left(\frac{\theta}{2}\right) \right\rangle$, $\bar{l}$ and $\overline{W}$ are mean values of sine of half of the tearing angle, the crack length and the width of flap over the simulation, respectively.

We have thus rationalized the two tearing regimes present in the data presented in Figure 3a of the main text. The first regime (at low adhesion strengths, $2 < \tau < 8$ J m^{-2}) is characterized by the scaling, $\sin\frac{\theta}{2} \propto \sqrt{\tau}$, and the contribution to the elastic energy is dominated by bending. In the second regime (at high adhesion strengths, $\tau > 8$ J m^{-2}), stretching dominates and the new scaling we arrived at in Equation (S14), $\sin\frac{\theta}{2} \propto \tau^2$, is observed.

Deformation fields as a function of adhesion energy

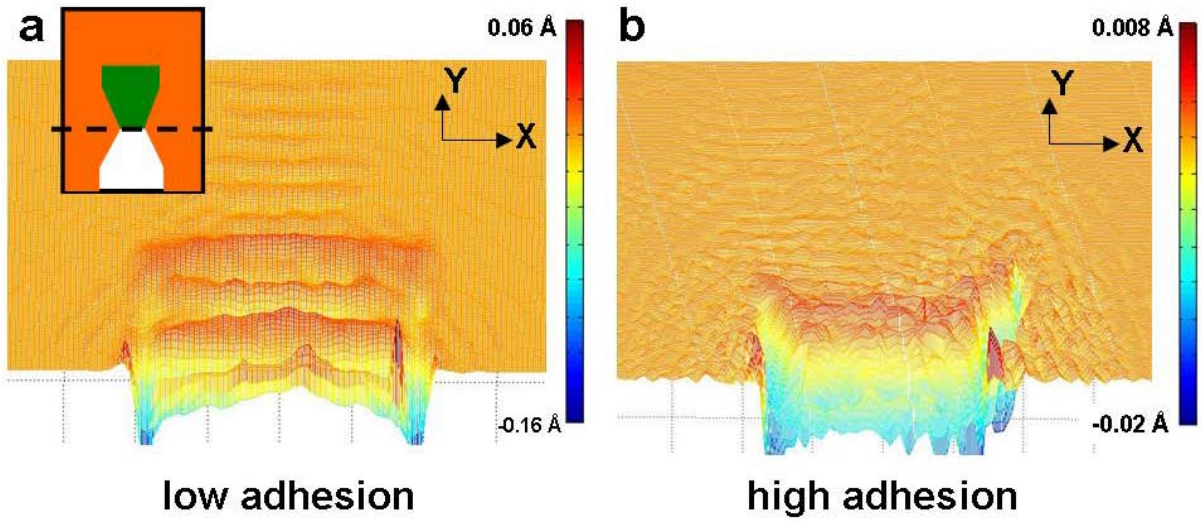

Figure S5. Surface plots of the out-of-plane (Z) deformation fields in the graphene sheet for (a) 'low' and (b) 'high' adhesion cases, as shown in Figure 4 in the main text, are calculated from molecular dynamics simulations. The inset in (a) shows a dotted line along which the view is cut off for ease of visualization and the viewing angle of the plots is in the XZ plane, at an angle to the Z axis. Out-of-plane displacements in the sheet ahead of the bent edge are seen for both cases, and the maximum gradients in the displacement (indicating local geometric torsion in the sheet) are seen to correspond to the high σ_{ZX} shear stress regions seen in the stress plots.

Graphene oxide

We have studied the flakes of graphene oxide, deposited on silicon oxide substrate. No tears, similar to those observed in graphene were found. Although the method for preparation and deposition of graphene oxide flakes (exfoliation of graphite oxide by agitation in water with subsequent spin-casting on the silicon oxide surface) does not necessarily facilitate the production of such tears (unlike that in graphene, which has been obtained by the micromechanical exfoliation), we suspect that the reason might be more fundamental and related to the very different mechanical properties of graphene oxide, and the defect and functionalization structure in the sheet.

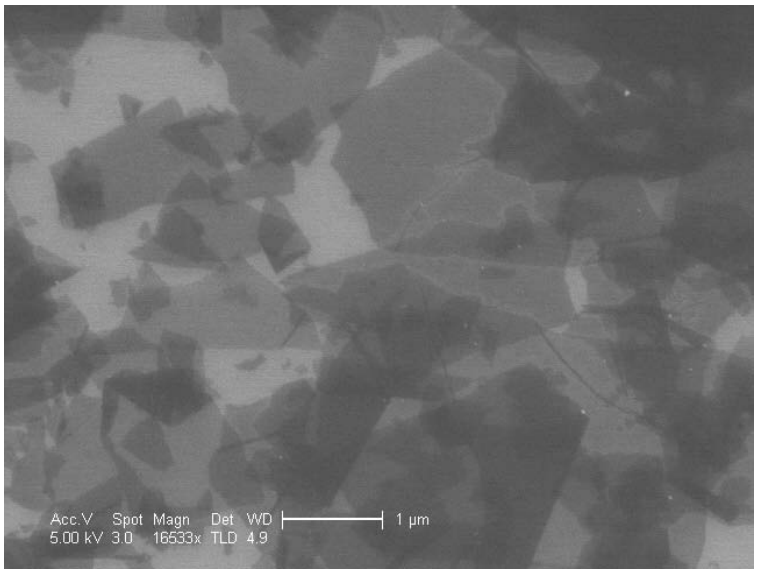

Figure S6. Flakes of graphene oxide as deposited from suspension on silicon oxide substrate by spin coating (SEM image). No tears, similar to those in graphene, have been observed.

Supplementary References

[47] B. R. Lawn, Fracture of Brittle Solids, Cambridge Univ. Press, 1993.
[48] Z. Suo, Applied Mechanics Reviews 1990, 43, S276.